

## Phase behavior of antiferromagnetic ultrathin magnetic films

A. M. Abu-Labdeh and J. P. Whitehead

*Department of Physics and Physical Oceanography, Memorial University of Newfoundland, St. John's, Newfoundland, Canada A1B 3X7*

K. De'Bell

*Department of Physical Science, University of New Brunswick at Saint John, Saint John, New Brunswick, Canada E2L 4L4*

A. B. MacIsaac

*Department of Applied Mathematics, University of Western Ontario, London, Ontario, Canada N6A 5B9*

(Received 16 March 2001; revised manuscript received 16 July 2001; published 19 December 2001)

The phase diagram of a system of classical spins on a square lattice, interacting through a nearest-neighbor antiferromagnetic exchange and a dipolar interaction, is presented. The phase diagram is based on results from a series of Monte Carlo simulations. The phase diagram shows a parallel antiferromagnetic phase, in which the spins are aligned in the  $x$ - $y$  plane, and an antiferromagnetic perpendicular phase, in which the spins are aligned perpendicular to the  $x$ - $y$  plane. The critical value of the exchange interaction,  $J_c(T)$ , on the phase boundary separating the two phases shows only a weak dependence on temperature ( $J_c \approx J_0$ ), while the transition appears to be first order with an extremely small latent heat. The Monte Carlo data also indicate that the parallel phase separates into two distinct phases, although further work is required to determine the precise nature of the phase boundary separating the two regions. Finally, the low-temperature magnetization data suggest a softening of the spin-wave stiffness close to the phase boundary. The Néel temperature of the perpendicular antiferromagnetic phase is found to be consistent with earlier predictions of spin-wave calculations.

DOI: 10.1103/PhysRevB.65.024434

PACS number(s): 75.70.Ak, 75.50.Ee, 75.30.Kz

### I. INTRODUCTION

Ultrathin magnetic films consist of a small number of monolayers of magnetic atoms deposited on a nonmagnetic substrate.<sup>1,2</sup> In many cases the magnetic moments are observed to order at low temperatures, and show a variety of ordered phases.<sup>3,4</sup> The magnetic properties of these films depend on the subtle interplay between the long-range anisotropic dipolar interaction, the short-range rotationally invariant exchange, and the magnetic surface anisotropy.

In this paper we examine the phase behavior that can arise as a consequence of the competition between dipolar and exchange interactions in low-dimensional antiferromagnetic systems. We do not, therefore, include the effect of the magnetic surface anisotropy, although the model could be easily extended to incorporate this into the analysis. Our study is based on results from Monte Carlo simulations of a simple model of antiferromagnetic thin films. The model consists of  $N$  classical spins of fixed length arranged on a square lattice of length  $L$  ( $L \times L = N$ ), which interact through a nearest-neighbor antiferromagnetic exchange interaction and a long-range dipolar interaction.

In this model the energy of a particular spin configuration  $\{\sigma_i\}$  is given by

$$E(\{\sigma_i\}) = -J \sum_{\langle ij \rangle} \vec{\sigma}_i \cdot \vec{\sigma}_j + g \sum_{i \neq j} \left( \frac{\vec{\sigma}_i \cdot \vec{\sigma}_j}{r_{ij}^3} - 3 \frac{(\vec{\sigma}_i \cdot \vec{r}_{ij})(\vec{\sigma}_j \cdot \vec{r}_{ij})}{r_{ij}^5} \right), \quad (1)$$

where  $\vec{\sigma}_i$  is a three-dimensional classical spin vector with  $\sigma^2 = 1$ . In the first term  $J$  is the strength of exchange interaction, and the sum is over all nearest-neighbor pairs  $\langle ij \rangle$ . A positive  $J$  corresponds to a ferromagnetic exchange interaction, while a negative  $J$  corresponds to an antiferromagnetic interaction. The second term of Eq. (1) represents a long-ranged dipole-dipole interaction, where the sum is over all possible pairs of the atoms in the lattice,  $\vec{r}_{ij}$  is the vector connecting site  $i$  to site  $j$ , and  $g$  denotes the strength of the dipolar interaction. Suitable boundary conditions are imposed on the system by constructing an infinite plane from replicas of a finite system, and using Ewald summation techniques to sum over the replicas. From this we can determine an effective interaction matrix for the finite system.<sup>5</sup>

In the absence of an exchange interaction ( $J=0$ ) the ground-state spin configuration has spins aligned in the plane of the film. However, it was noted by several authors that the planar ground state of the pure dipolar system is continuously degenerate.<sup>6-8</sup> Two examples of dipolar ground-state spin configurations are shown in Figs. 1(a) and 1(b). Other ground-state spin configurations can be generated by a transformation which continuously maps the spin configuration shown in Fig. 1(a) into the spin configuration shown in Fig. 1(b) by varying the angle  $\phi$  shown in Fig. 2.<sup>8</sup> The fact that the ground state is continuously degenerate is somewhat surprising, since the dipolar interaction is not invariant under rotation. It can readily be shown that the energy of these states is not affected by the addition of the exchange interaction, and is given by<sup>5</sup>

$$E_{\parallel} = -5.0989g. \quad (2)$$

For low values of  $|J|$ , this manifold of degenerate states

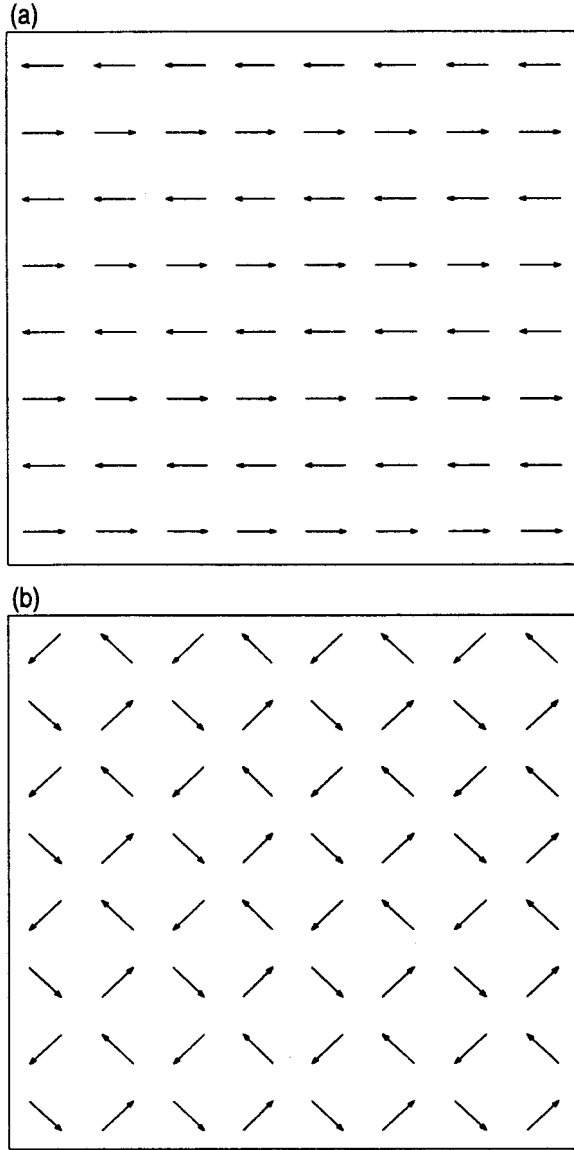


FIG. 1. Two planar ground-state spin configurations. In one (a), the spins are aligned along the  $x$  axis. In the other (b), they are oriented at  $\pm \pi/4$  to the  $x$  axis.

constitutes the ground state. However, if the strength of the antiferromagnetic exchange parameter is sufficiently large, the ground-state spin configuration switches to one in which the spins are perpendicular to the plane of the film, with each spin aligned antiparallel to each of its nearest neighbors. The energy of this state,  $E_{\perp}$ , is given by<sup>5</sup>

$$E_{\perp} = -2.6459g - 2|J|. \quad (3)$$

Comparing the energies of the planar spin configuration [Eq. (2)] and the perpendicular phase [Eq. (3)], it is seen that, at zero temperature, a transition from a degenerate parallel antiferromagnetic phase to a nondegenerate perpendicular antiferromagnetic phase occurs when  $|J| = J_0$ , with

$$J_0/g = (5.0989 - 2.6459)/2 = 1.2265 \quad (4)$$

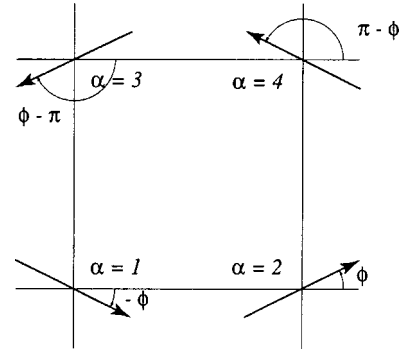


FIG. 2. A schematic of the magnetic unit cell used to describe the magnetic order showing the four magnetic sublattices and labels attached to them. The energy of the spin configuration is independent of the angle  $\phi$  shown in the figure.

Thus we see that the competition between dipolar and antiferromagnetic exchange interactions can give rise to a reorientation transition.

To construct order parameters for both of these states, we divide the lattice into four sublattices, each of which is square, with a lattice spacing twice that of the original lattice.<sup>8</sup> The magnetic lattice therefore contains four sites per unit cell, each site corresponding to one of the sublattices. Denoting the four sites by  $\alpha \in \{1 \dots 4\}$ , as shown in Fig. 2, we define the sublattice magnetizations  $\vec{M}_{\parallel}^{\alpha}$  and  $M_{\perp}^{\alpha}$  as

$$\vec{M}_{\parallel}^{\alpha} = \frac{4}{N} \left( \sum_{\vec{r}_{\alpha}} \sigma^x(\vec{r}_{\alpha}) \right) \hat{x} + \frac{4}{N} \left( \sum_{\vec{r}_{\alpha}} \sigma^y(\vec{r}_{\alpha}) \right) \hat{y} \quad (5)$$

and

$$M_{\perp}^{\alpha} = \frac{4}{N} \sum_{\vec{r}_{\alpha}} \sigma^z(\vec{r}_{\alpha}), \quad (6)$$

from which we define the order parameters  $M_{\parallel}$  and  $M_{\perp}$  as

$$M_{\parallel} = \frac{1}{4} \sum_{\alpha=1}^4 |\vec{M}_{\parallel}^{\alpha}|, \quad (7)$$

$$M_{\perp} = \frac{1}{4} \sum_{\alpha=1}^4 |M_{\perp}^{\alpha}|. \quad (8)$$

For the planar ground state  $|J| < J_0$ , we have

$$M_{\parallel} = 1,$$

$$M_{\perp} = 0,$$

while for the perpendicular ground  $|J| > J_0$  we have

$$M_{\parallel} = 0,$$

$$M_{\perp} = 1.$$

In the following sections we discuss the finite-temperature properties of the model, and present the results of the simulations including the phase diagram. A brief discussion of the

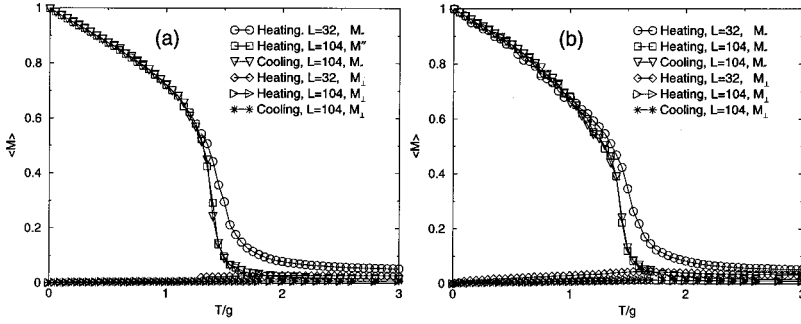


FIG. 3. A plot of the perpendicular and parallel order parameters  $M_{\perp}$  and  $M_{\parallel}$  as a function of  $T/g$  for (a)  $|J|=0.4g$  and (b)  $|J|=1.0g$  for  $L=32$  and 104.

low-temperature order parameter follows, and we finish the paper with a discussion of some potential applications of the results.

## II. FINITE-TEMPERATURE PROPERTIES

In the case of the pure dipolar system ( $J=0$ ), Monte Carlo simulations clearly show the existence of long-range magnetic order for both planar<sup>8,9</sup> and the Heisenberg<sup>10</sup> models at low temperature. In both cases the equilibrium spin configuration is antiferromagnetic, with the spins aligned along the  $x$  or  $y$  axis, similar to the configuration shown in Fig. 1(a). Since the dipolar ground state is continuously degenerate, the existence of long-range magnetic order poses two interesting and subtle questions, both of which are relevant to the current work. First, since the degeneracy of the ground state implies the existence of a gapless mode in the spin-wave spectra, a result confirmed by spin-wave calculations for both the Heisenberg<sup>11</sup> and the planar<sup>8</sup> models, why does the amplitude of spin fluctuations not diverge and the magnetic order disappear at finite temperature? Second, if the long-range magnetic order does persist at finite temperature, how is the easy axis of magnetization determined if the ground state is continuously degenerate?

The answer to both these questions lies in the fact that the degeneracy of the dipolar ground state does not arise as a result of a global symmetry. As a consequence, while the ground-state energy is independent of the magnetization axis, the spectrum of energy excitations is not. This means that thermal spin fluctuations break the degeneracy of the ground state, and generate an effective potential that has the fourfold symmetry of the underlying lattice.<sup>8,12,13</sup> This effective potential will manifest itself as a gap in the spin-wave spectra<sup>9,14</sup> that renders the amplitude finite, but singular,<sup>9</sup> at finite temperature, and which will serve to define an easy axis of magnetization.

A similar situation pertains in the case of the present model for  $|J| < J_0$ . Shown in Fig. 3, for  $|J|=0.4g$  and  $|J|=1.0g$ , are the order parameters  $M_{\parallel}$  and  $M_{\perp}$  defined by Eqs. (8) and (7), but in terms of the thermally averaged sublattice magnetization:

$$\vec{M}_{\parallel}^{\alpha} = \frac{4}{N} \left\langle \sum_{\vec{r}_{\alpha}} \sigma^x(\vec{r}_{\alpha}) \right\rangle \hat{x} + \frac{4}{N} \left\langle \sum_{\vec{r}_{\alpha}} \sigma^y(\vec{r}_{\alpha}) \right\rangle \hat{y} \quad (9)$$

and

$$M_{\perp}^{\alpha} = \frac{4}{N} \left\langle \sum_{\vec{r}_{\alpha}} \sigma^z(\vec{r}_{\alpha}) \right\rangle. \quad (10)$$

In both cases the data show a planar phase at low temperatures  $M_{\parallel} \neq 0$  and  $M_{\perp} \approx 0$ . As the temperature is increased the order parameter decreases, dropping rapidly at around  $T/g = 1.4 \pm 0.05$  for both  $|J|=0.4g$  and  $|J|=1.0g$ , indicating a transition from an ordered planar antiferromagnetic phase to a disordered paramagnetic phase. In both cases the data show the transition sharpening as the system size increases, consistent with a second-order transition. The existence of a second-order phase transition is also reflected in the heat capacity (Fig. 4) and the susceptibility of the sublattice magnetization (Fig. 5). It is interesting to note that, while the equilibrium phase at low temperature clearly shows a long-range magnetic order, the heat capacity for the planar phase shows a transition that is relatively insensitive to the system size. Qualitatively the peak in the heat capacity resembles the peak in the heat capacity at the Kosterlitz-Thouless transition in the two-dimensional  $X$ - $Y$  model ( $g=0$ ).

While the order parameter, specific heat, and other thermodynamic observables appear qualitatively similar for different values of  $J$  (Figs. 3–5) the nature of the equilibrium spin configurations are nevertheless quite different. A sample

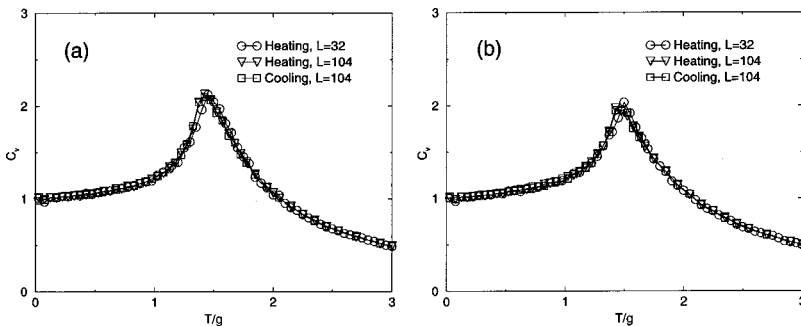


FIG. 4. A plot of the heat capacity per spin as a function of temperature for (a)  $|J|=0.4g$  and (b)  $|J|=1.0g$  for  $L=32$  and 104.

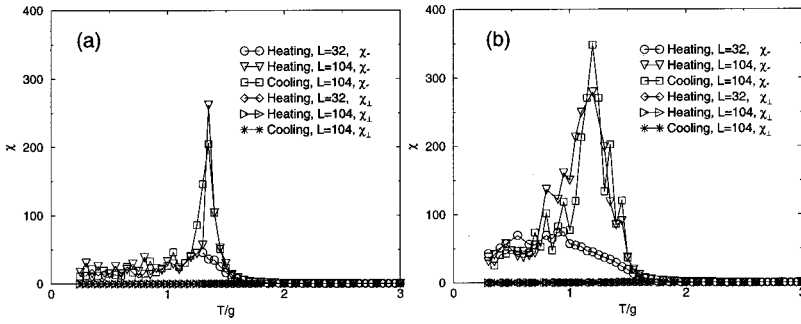


FIG. 5. A plot of the perpendicular and parallel susceptibilities  $\chi_{\perp}$  and  $\chi_{\parallel}$  as a function of temperature for (a)  $|J|=0.4g$  and (b)  $|J|=1.0g$  for  $L=32$  and  $104$ .

spin configuration for each value of  $J$  is shown in Fig. 6 for  $T=0.15g$ . The spin configuration in Fig. 6(a) shows quite clearly that the sublattice magnetization for  $|J|=0.4g$  is similar to that for the pure dipolar system,  $J=0$ , with the spins aligned along the  $x$  or  $y$  axis. In contrast, the spin configuration in Fig. 6(b) shows that for  $|J|=1.0g$  the

sublattice magnetization is oriented at  $\pi/4$  to the  $x$  and  $y$  axes. This implies that two distinct ordered planar phases exist.

The difference in the orientation of the equilibrium spin configuration is also apparent in Fig. 7, which shows the angles  $\theta_{\alpha}$  as a function of the temperature  $T$  for two values of  $J$ , where the angles  $\theta_{\alpha}$  are defined for each of the sublattices as

$$\theta_{\alpha} = \arctan\left(\frac{M_y^{\alpha}}{M_x^{\alpha}}\right). \quad (11)$$

The data are presented for cooling, and show at high temperature that the spins on each of the four sublattices do not appear to exhibit any preferred orientation within the plane for both  $|J|=0.4g$  and  $1.0g$ . As the temperature is lowered and the antiferromagnetic order is established, the spins in each of the magnetic sublattices begin to order along one of the symmetry axes. However, it is apparent from the data that the symmetry axis is different for different values of  $|J|$ . For  $|J|=0.4g$  the symmetry axis is along the  $x$  axis, with  $\theta_1 = \theta_2 = 0$  and  $\theta_3 = \theta_4 = \pi$ , while for  $|J|=1.0g$  the symmetry axis is oriented at  $\pi/4$  to the  $x$  axis with  $\theta_1 = \pi/4$ ,  $\theta_2 = 3\pi/4$ ,  $\theta_3 = 5\pi/4$ , and  $\theta_4 = 7\pi/4$ .

For  $|J| > J_0$  the ground-state spin configuration has spins aligned perpendicular to the plane of the film. Shown in Fig. 8(a), for  $|J|=2.0g$ , are the order parameters  $M_{\parallel}$  and  $M_{\perp}$  defined by Eqs. (8) and (7), calculated using the thermally averaged sublattice magnetization. The corresponding heat capacity is shown in Fig. 8(b). The data show a perpendicular antiferromagnetic phase, with each spin aligned antiparallel to its nearest neighbor. As the temperature is increased the order parameter decreases, dropping rapidly at around  $T/g = 2.5 \pm 0.05$  for  $|J|=2.0g$ , indicating a transition from an ordered perpendicular antiferromagnetic phase to a disordered paramagnetic phase. As with the parallel phase discussed above, the order parameter data show the transition sharpening as the system size increases, consistent with a second-order transition. Comparing the heat capacity of Fig. 8(b) for the perpendicular phase with that shown in Fig. 4 for the parallel phase, it is worth noting that the peak in the heat capacity for the perpendicular phase shows a more pronounced size effect.

The transition from the a planar antiferromagnetic phase to a perpendicular antiferromagnetic phase is clearly seen in Figs. 9, 10, and 11, which show how the order parameters  $M_{\parallel}$  and  $M_{\perp}$  (Fig. 9), the total internal energy (Fig. 10), and the dipolar and exchange energies (Fig. 11) change with in-

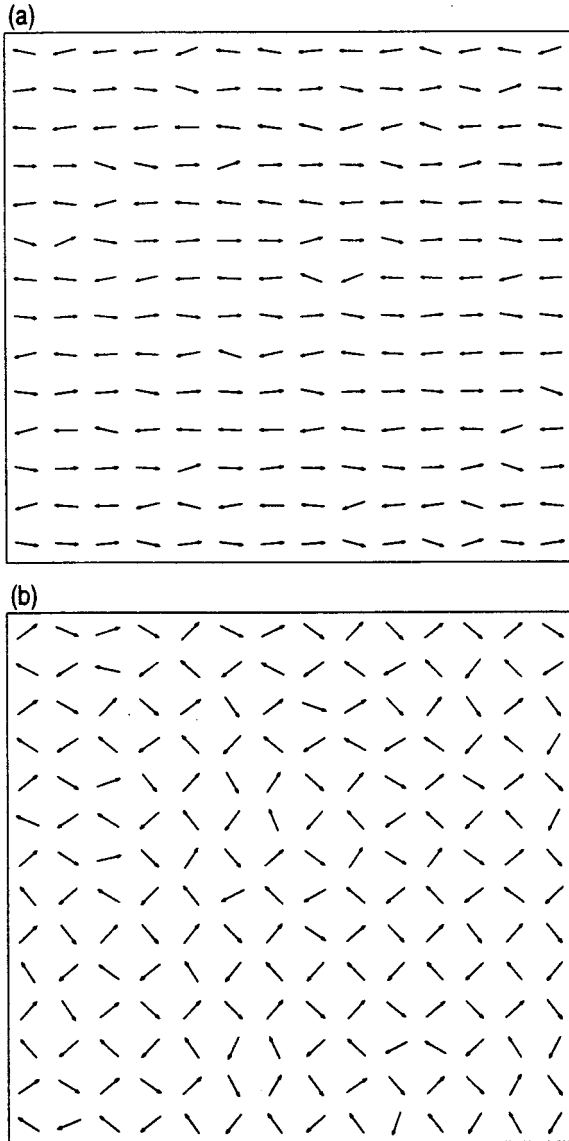


FIG. 6. Snapshots of two typical spin configurations at  $T=0.15g$  (a)  $|J|=0.4g$  and (b)  $|J|=1.0g$ .

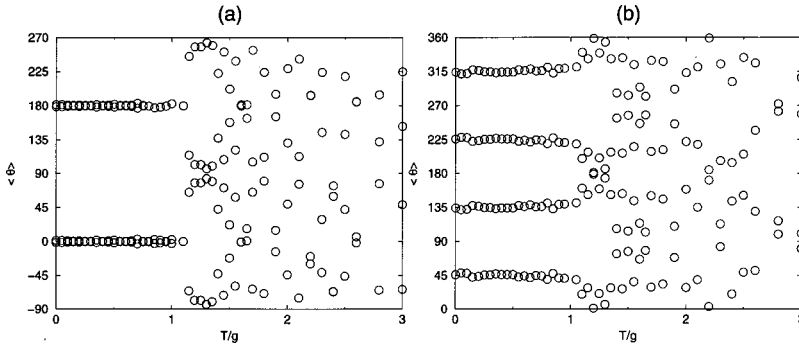


FIG. 7. A plot of the angle  $\theta_\alpha$  as a function of decreasing temperature,  $T/g$ , for (a)  $|J|=0.4g$  and (b)  $|J|=1.0g$  for  $L=104$ .

creasing  $|J|$  for  $T=0.4g$ . It is worth noting that while the data indicate that the transition from a planar phase to a perpendicular antiferromagnetic phase is first order, the latent heat at the transition is very small. Instead the transition is characterized by a sharp change in the slope of the energy with respect to  $|J|$ . The discontinuous nature of the transition is more clearly seen in Fig. 11, in which the exchange and dipolar energies are plotted with increasing  $|J|$ . The curves show that in the planar phase ( $|J| < |J_0|$ ) the energy of the system is almost entirely dipolar,  $E_{\text{ex}} \approx 0$ . At the transition  $|J| = (1.226 \pm 0.02)g$ , the system switches from a planar phase to a perpendicular phase, and the exchange energy is seen to decrease abruptly and the dipolar energy to increase. The data also show a small amount of hysteresis, consistent with the discontinuous nature of the transition.

Further evidence of the transition between the two planar phases is also seen in the susceptibilities of the sublattice magnetization, shown in Fig. 12, which show not one peak but two distinct peaks. The first peak, at  $|J|=0.69g$ , corresponds to the reorientation transition from one planar phase to the other, and the second peak to the transition from a planar phase to a perpendicular phase.

### III. PHASE DIAGRAM

The phase diagram constructed from the Monte Carlo data is shown in Fig. 13. The graph shows the three phase boundaries separating the perpendicular antiferromagnetic phase (region II), the planar antiferromagnetic phase (region I), and the paramagnetic phase (region III). The dotted line in region I indicates the phase boundary separating the two planar phases. The precise natures of this boundary and its location are tentative.

The phase boundary separating the planar and perpendicular antiferromagnetic phases appears, from the Monte

Carlo (MC) data, to be first order. The order parameters  $M_\perp$  and  $M_\parallel$  change abruptly with increasing and decreasing  $|J|$ , and the data show a small amount of hysteresis. While the transition between perpendicular and parallel antiferromagnetic phases appears to be first order, the latent heat of the transition is relatively small along the length of the phase boundary. This is consistent with the observation that the phase boundary separating regions I and II is almost horizontal. Letting  $J_c(T)$  define the phase boundary, it can be readily shown (see the Appendix) that the slope of the coexistence line  $dJ_c/dT$  is proportional to the latent heat  $l$ , and is given by

$$\frac{dJ_c}{dT} = \frac{Jl}{T\Delta U_{\text{ex}}}, \quad (12)$$

where  $\Delta U_{\text{ex}}$  denotes the difference in the exchange energy between the equilibrium phases on the coexistence line. Preliminary estimates of the slope and the latent heat are consistent with this result, although the range of the uncertainty is relatively large making a precise confirmation of this result difficult.

The phase boundary separating the perpendicular antiferromagnetic phase from the paramagnetic phase is determined by the peak position in the heat capacity of the system. Size effects, the continuous decrease in the order parameter, and the lack of any hysteresis suggest that this phase boundary defines a line of second-order transitions. This is consistent with the theoretical results of Pich and Schwabl.<sup>15</sup> Based on a generalized spin-wave theory Pich and Schwabl obtained the following relationship for the Néel temperature  $T_N$  for  $|J| \gg g$  (Ref. 15):

$$\frac{|J|}{T_N} = a \ln\left(\frac{|J|}{g}\right) + b. \quad (13)$$

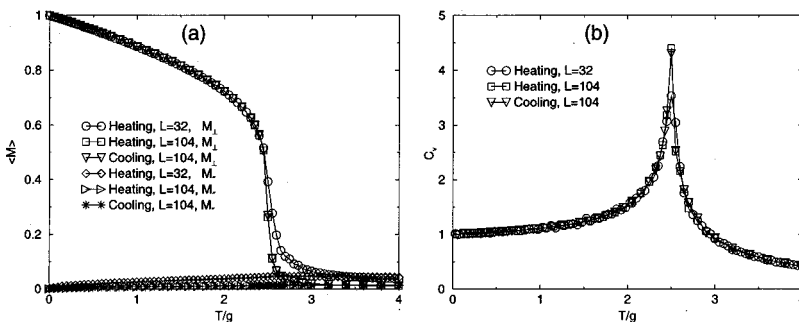


FIG. 8. A plot of the (a) perpendicular and parallel order parameters  $M_\perp$  and  $M_\parallel$ , and (b) the heat capacity per spin as a function of temperature for  $|J|=2.0g$  with  $L=32$  and  $104$ .

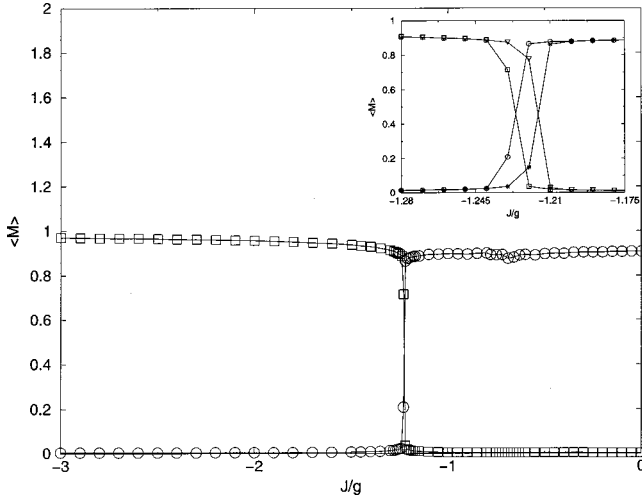


FIG. 9. A plot of the parallel (○) and perpendicular (□) order parameters  $M_{\perp}$  and  $M_{\parallel}$  as a function of  $J/g$  for  $T=0.4g$  and  $L=104$  increasing  $|J|$ . [Inset: (○)  $M_{\perp}$  and (□)  $M_{\parallel}$  with  $|J|$  increasing and (▽)  $M_{\perp}$  and (\*)  $M_{\parallel}$  with  $|J|$  decreasing.]

To compare this relationship with the results of the Monte Carlo calculation, we plot  $\log(|J|/g)$  as a function of  $|J|/T_N$  in Fig. 14. From this figure we see that the MC data do indeed fall on straight line for large values of  $|J|/g$  as predicted by Pich and Schwabl.<sup>15</sup> The solid line shown in the figure is the line of best fit for the points  $|J| > 2.0g$ . The equation for the best fit line gives  $a=0.1963$  and  $b=0.6599$ .

The phase boundary separating the planar antiferromagnetic (AF) phase from the paramagnetic phase is also shown, and, again, appears to describe a line of second-order phase transitions. We are not yet aware of any theoretical results for the Néel temperature for the planar AF phase with which to compare our results.

The dotted line on the phase diagram represents the boundary between the two in-plane phases. For this study the boundary was determined from the corresponding peak in the parallel susceptibility and, based on the results from the simulations, we tentatively identify the transition as a discontinuous first-order transition.

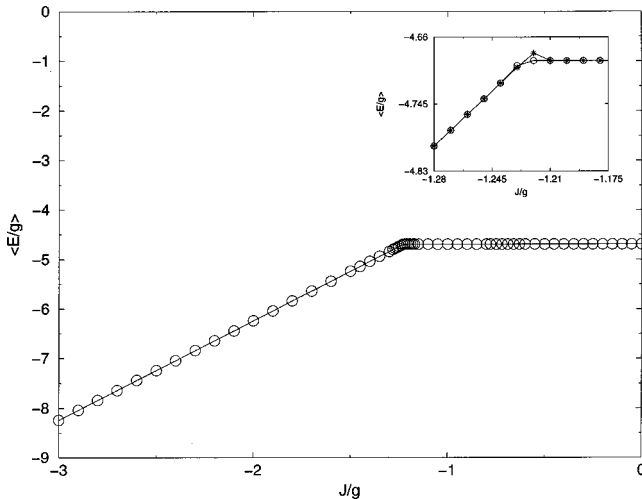


FIG. 10. A plot of the internal energy per spin as a function of  $J/g$  [(○) increasing  $|J|$  and (\*) decreasing  $|J|$ ] for  $T=0.4g$  and  $L=104$ .

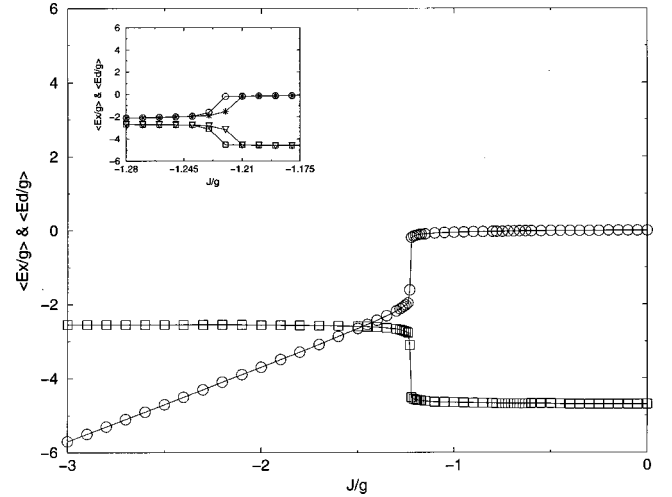


FIG. 11. A plot of the exchange energy [(○) for increasing  $|J|$  and (\*) for decreasing  $|J|$ ] and the dipolar energy [(□) increasing  $|J|/g$  and (▽) decreasing  $|J|/g$ ] per spin as a function of  $J/g$  for  $T=0.4g$  and  $L=104$ .

#### IV. LOW-TEMPERATURE ORDER PARAMETER

While the simulations are consistent with a first-order transition from the perpendicular phase to the parallel AF phase with decreasing  $|J|$ , the low-temperature order-parameter data indicate a significant softening of the spin-wave spectra as the transition is approached. In Fig. 15 the perpendicular order parameter is plotted as a function of  $T$  for several values of  $|J| > J_0$ . The graphs show that the perpendicular order parameter decreases linearly with increasing temperature as  $T \rightarrow 0$ . The linear decrease of the order parameter with temperature may be readily understood on the basis of classical linear spin-wave theory. The magnitude of the sublattice magnetization  $m^{\alpha}$  may be written as

$$m^{\alpha} \equiv \left| \frac{4}{N} \sum_{r_{\alpha}} \vec{\sigma}(r_{\alpha}) \right| = 1 - \frac{4}{N} \sum_{r_{\alpha}} \langle b^{*}(r_{\alpha}) b(r_{\alpha}) \rangle \quad (14)$$

where  $b(r_{\alpha})$  denotes the complex amplitude associated with the spin fluctuations at a site  $r_{\alpha}$  in the  $\alpha$  sublattice. At low temperature the thermal average  $\langle b^{*}(r_{\alpha}) b(r_{\alpha}) \rangle$  may be calculated from linear spin-wave theory, provided the spin-wave spectrum is not gapless. It can readily be shown that  $\langle b^{*}(r_{\alpha}) b(r_{\alpha}) \rangle \propto T$ ; however, due to the presence of the dipolar interaction, the proportionality constant is quite difficult to calculate in general. It is clear from the graphs shown in Fig. 15 that the slope of the perpendicular order parameter in the limit  $T \rightarrow 0$  decreases with decreasing  $|J|/g$ , reflecting a softening of the spin-wave stiffness.

A plot of  $\lim_{T \rightarrow 0} |dM/dT|$ , as a function of  $|J|/g$  is shown in Fig. 16. The dependence of  $\lim_{T \rightarrow 0} |dM/dT|$  on the exchange parameter, shown in Fig. 16, shows a rapid increase in the magnitude as the transition is approached. The figure shows a comparison with a phenomenological relationship

$$\lim_{T \rightarrow 0} \frac{|dM|}{|dT|} = \frac{a}{((|J|/g)^b - c)^d}, \quad (15)$$

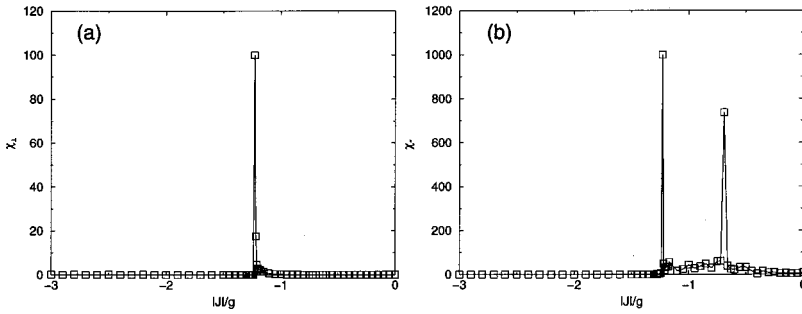


FIG. 12. A plot of the perpendicular and parallel susceptibilities  $\chi_{\perp}$  (a) and  $\chi_{\parallel}$  (b) as a function of  $J_g$  for  $T=0.4g$  and  $L=104$  ( $|J|$  increasing). Both the perpendicular and parallel susceptibilities exhibit peaks at the in-plane to out-of-plane transition. The parallel susceptibility exhibits a second peak corresponding to the in-plane reorientation transition.

where a regression analysis yields the following estimates  $a=0.166$ ,  $b=2.38348$ ,  $c=1.49$ , and  $d=0.316508$ . This relationship predicts that the slope of the order parameter diverges at  $|J|/g=1.1805$ , which lies just below the phase boundary separating the perpendicular and in-plane phases.

A similar analysis of the order parameter in the parallel phase is complicated by the fact that the temperature dependence of the sublattice magnetization appears to deviate systematically from a linear behavior at low temperature. This is due to a gapless branch in the spin-wave spectra that arises as a consequence of the degeneracy of the ground state. In Fig. 17 we plot  $g(1-M_{\parallel})/T$  vs  $T/g$  for  $|J|=0.2g$ . We see that the points do not tend to a constant in the limit  $T \rightarrow 0$ , as expected from linear spin-wave theory, but, instead, show a steady increase as the temperature is reduced. This is consistent with the results of Carboognani *et al.*<sup>9</sup> for the planar model, and suggests that the degeneracy of the planar ground state also manifests itself in the case of the Heisenberg model by a nonanalytical temperature dependence in the order parameter at  $T=0$ .

V. DISCUSSION

Antiferromagnetic ultrathin magnetic films are interesting for a variety of reasons, not least because the competition

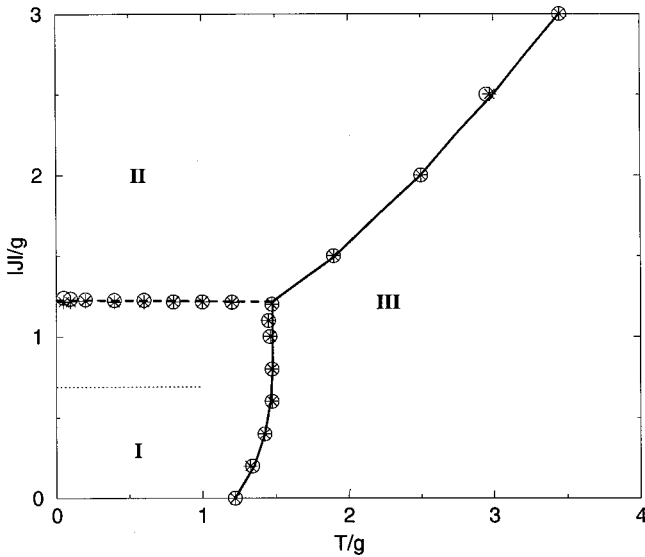


FIG. 13. The phase diagram for the antiferromagnetic dipolar system, as a function of  $|J|/g$  and  $T/g$ . The three phases are: I in plane antiferromagnetically ordered, II out of plane antiferromagnetically ordered, and III disordered. The dotted line separates the two planar phases [ $L=104$ , (O) for increasing  $|J|$  and  $T$ , and (\*) for decreasing  $|J|$  and  $T$ ].

between the antiferromagnetic exchange and the dipolar interaction is sufficient to induce a reorientation from an in-plane phase to a perpendicular phase. The results from the simulations show that the function  $J_c(T)$ , that describes the phase boundary between the planar and perpendicular antiferromagnetic phases, is only weakly dependent on the temperature, suggesting that the effective anisotropy that arises as a consequence of the exchange and the dipolar interaction is largely independent of temperature. To what extent this result will be modified by the addition of an explicit magnetic surface anisotropy is not at all obvious, and is currently under investigation.

A subtle aspect of the phase behavior arises from the degeneracy of the planar ground-state energy. The existence of long-range magnetic order and the orientation of the easy axis of magnetization is determined by the disorder produced by the thermal fluctuations. This provides an explicit example of the concept of “order from disorder” discussed by Henley.<sup>12</sup> Indeed Henley<sup>12</sup> and Prakash and Henley<sup>13</sup> showed that the orientation of the magnetization axis generated by disorder is critically dependent on the precise nature of the disorder. In particular, in the case of an antiferromagnetic X-Y model, the effective potential arising as a consequence of the thermal fluctuations has minima on the  $x$ - $y$  axis, while the disorder arising from the effects of dilution has minima at  $\pm \pi/4$  to the  $x$ - $y$  axis. It seems reasonable, on the basis of the work by Henley and co-workers, to assume that it is the change in the nature of the disorder, as the exchange interaction  $|J|$  is increased, that gives rise to the reorientation

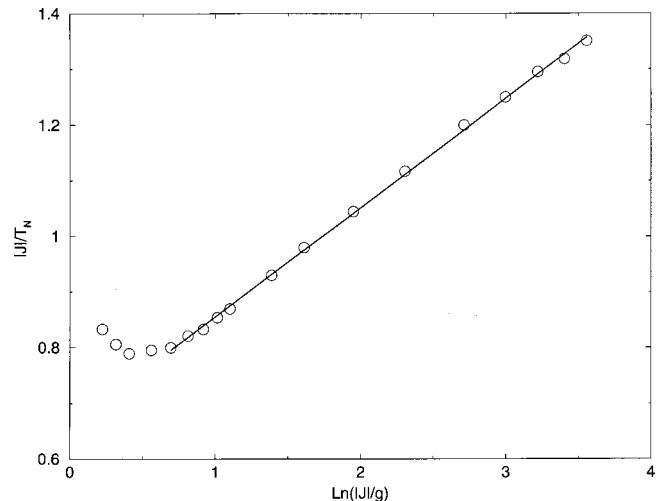


FIG. 14. A plot of  $|J|/T_N$  vs  $\log|J|/g$  for  $|J| > J_0$ .

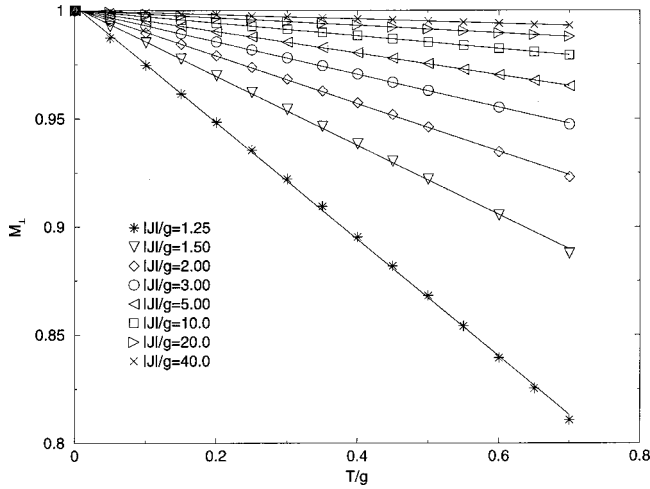


FIG. 15. A plot of the perpendicular order parameter  $M_{\perp}$  as a function of increasing temperature ( $T/g$ ), for several values of  $|J| > J_0$ .

transition within the planar phase which is observed in these simulations.

A further motivation to determine how thermal fluctuations can give rise to an in-plane reorientation transition is provided by a recent experimental observation of such a plane transition in a ferromagnetic system.<sup>16</sup> While it by no means obvious how the results obtained in this study are relevant to the ferromagnetic case, it is possible that both arise as a consequence of the same underlying physical process.

The simulations also lend support to some predictions of nonlinear spin-wave theory. In particular, the Néel temperature for the perpendicular phase appears to be consistent with the results of Pich and Schwabl,<sup>15</sup> while an analysis of the low-temperature magnetization in the planar phase shows a singularity qualitatively similar to that predicted by Carbogiani *et al.*<sup>9</sup> for a planar model in the absence of an exchange interaction. Obviously a more quantitative comparison between spin-wave theory and the results obtained from simu-

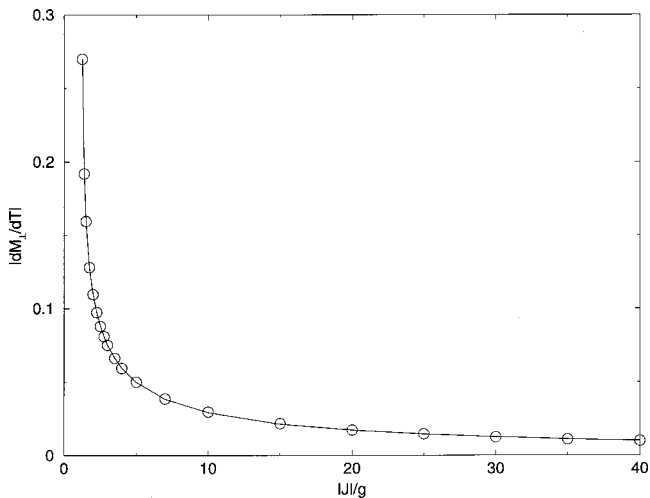


FIG. 16. A plot of the slope  $\lim_{T \rightarrow 0} dM_{\perp}/dT$  as a function of the exchange interaction  $|J|/g$ , for  $|J| > J_0$ .

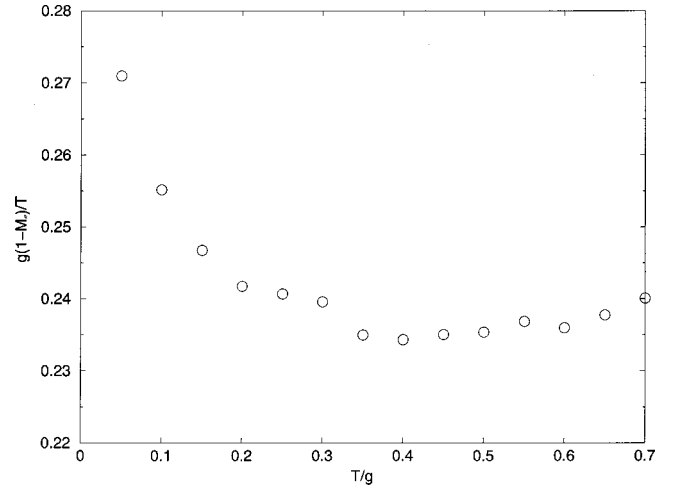


FIG. 17. A plot of ratio  $(1 - M_{\parallel})/T$  as a function of  $T/g$ , for  $|J| < J_0$ . Note that the ratio increases as  $T \rightarrow 0$ . Linear spin-wave theory predicts that  $\lim_{T \rightarrow 0} (1 - M_{\parallel})/T = \text{const}$ .

lations would be useful, and could include an analysis of the low-temperature magnetization in the perpendicular phase to examine the spin-wave spectra close to the phase boundary and the effect of excitations on the magnetization.

One important class of quasi-two-dimensional antiferromagnetic materials in which the dipolar energy is comparable to the exchange energy are the so called High- $T_c$  superconductors  $R\text{Ba}_2\text{Cu}_3\text{O}_{7-\delta}$  ( $R$  = rare earth). The structure of these compounds is such that the rare-earth ions reside on well-separated planes, replacing the yttrium (Y) ions of the parent compound  $\text{YBa}_2\text{Cu}_3\text{O}_{7-\delta}$ . The compounds in which dysprosium (Dy), gadolinium (Gd), or erbium (Er) are substituted for yttrium have been the most extensively studied.<sup>5</sup> At low temperature the spins are aligned perpendicular to the plane in the case of Dy (Ref. 17) and Gd (Ref. 18) compounds, and parallel to the planes in the case of Er compounds.<sup>19</sup>

The compound  $\text{GdBa}_2\text{Cu}_3\text{O}_{7-\delta}$  is of particular interest in the context of the present discussion since, as an  $S$ -wave ion, the crystalline electric field (CEF) anisotropy will disappear to leading order and, based on a simple scaling argument,<sup>5</sup> it will have the strongest exchange interaction of the three compounds. Therefore application of our model to this compound would locate the low-temperature phase of  $\text{GdBa}_2\text{Cu}_3\text{O}_{7-\delta}$  in region II of the phase diagram shown in Fig. 13. This is consistent with experimental observations of the order parameter and, while the observed low-temperature heat capacity is complicated by the quantum nature of the spins at low temperature, measurements nevertheless show a sharp peak at the transition similar to that presented in Fig. 8.<sup>20</sup>

More intriguing is the case of  $\text{ErBa}_2\text{Cu}_3\text{O}_{7-\delta}$ . According to the simple scaling argument referred to above, the Er compound will have the weakest exchange interaction of the three compounds [ $J(\text{Er}) \approx J(\text{Gd})/9$ ]. This is consistent with the fact that the moments are aligned in-plane at low temperature. In the case of the orthorhombic, superconducting phase of  $\text{ErBa}_2\text{Cu}_3\text{O}_{7-\delta}$  ( $\delta > 1/2$ ), the Er ions clearly order at low temperature along the the  $a$  axis, with the spins ordering

as shown in Fig. 1(a),<sup>19</sup> while the specific heat shows a sharp cusp at the Néel temperature.<sup>21</sup> In the tetragonal, insulating phase ( $\delta < 1/2$ ) the specific heat is much more rounded, and there does not appear to be any long-range magnetic order at low temperature.<sup>22</sup> Calculations of the CEF and the ground state of the Er ions show that, while the small orthorhombic distortion defines an easy axis of magnetization in the superconducting phase, in the tetragonal phase the magnetic moment of the Er ion is free to rotate in the plane.<sup>23</sup> While it is possible to argue that the rounded heat capacity observed experimentally is qualitatively similar to the heat capacity shown in Fig. 4, it is difficult to reconcile the absence of long-range magnetic order with the results presented here. A possible explanation of the absence of an observed ordered state is that the highly degenerate nature of the planar equilibrium phases, and the critical dependence of their stability on the nature of the disorder created by both the thermal fluctuations and any structural disorder (e.g. oxygen vacancies), results in frustration effects. These effects would prevent the system from realizing long-range magnetic order. Indeed, it is possible that such effects would produce a glass-like phase of microdomains that would be difficult to identify experimentally.

While the properties of the  $\text{GdBa}_2\text{Cu}_3\text{O}_{7-\delta}$  and  $\text{ErBa}_2\text{Cu}_3\text{O}_{7-\delta}$  compounds are consistent with certain aspects of the phase diagram shown in Fig. 13, a more complete picture of the magnetic properties of these compounds, and the others in this class, should include the magnetic anisotropy arising from the CEF and the effects of impurities.

#### ACKNOWLEDGMENTS

This work was supported, in part, by the Natural Sciences and Engineering Research Council of Canada. The authors gratefully acknowledge access to computational resources at The University of Calgary, provided under the auspices of C3.ca. One of the authors (J.P.W.) would also like to acknowledge the hospitality of the Department of Applied Mathematics at the University of Western Ontario, while this work was in progress and in particular numerous useful discussions with Dr. P. Poole.

#### APPENDIX

The free energy for a given value of the exchange constant  $J$  and temperature  $T$ ,  $F(J, T)$  may be written in terms of the energy  $E$  given by Eq. (1):

$$F = -T \log \sum_{\{\sigma_i\}} e^{-E(\{\sigma_i\})/T}. \quad (\text{A1})$$

From the energy given in Eq. (1), we obtain the following expression for the variation in the ratio  $F/T$  induced by a variation in the exchange constant  $J$  and the temperature  $T$ . Consider

$$\begin{aligned} d\left(\frac{F}{T}\right) &= \left(\frac{1}{T} \frac{\partial F}{\partial T} - \frac{F}{T^2}\right) dT + \frac{1}{T} \frac{\partial F}{\partial J} dJ \\ &= -\frac{1}{T} \left(\frac{ST-F}{T} dT - \frac{U_{\text{ex}}}{J} dJ\right) \\ &= -\frac{1}{T} \left(\frac{U}{T} dT - \frac{U_{\text{ex}}}{J} dJ\right). \end{aligned} \quad (\text{A2})$$

Let us consider two states which we label  $a$  and  $b$ , respectively. We have that

$$d\left(\frac{F^{(a)}}{T}\right) = -\frac{1}{T} \left(\frac{U^{(a)}}{T} dT - \frac{U_{\text{ex}}^{(a)}}{J} dJ\right), \quad (\text{A3})$$

$$d\left(\frac{F^{(b)}}{T}\right) = -\frac{1}{T} \left(\frac{U^{(b)}}{T} dT - \frac{U_{\text{ex}}^{(b)}}{J} dJ\right). \quad (\text{A4})$$

Subtracting, we obtain

$$d\left(\frac{\Delta F}{T}\right) = -\frac{1}{T} \left(\frac{\Delta U}{T} dT - \frac{\Delta U_{\text{ex}}}{J} dJ\right). \quad (\text{A5})$$

At the phase boundary separating the planar and perpendicular phases the two phases coexist and have the same free energy. Therefore, along the phase boundary we have  $\Delta F/T=0$ , and therefore  $d(\Delta F/T)=0$ , from which we obtain the following relationship for the difference between the exchange energy and the total energy of the two phases:

$$\frac{\Delta U}{T} dT = \frac{\Delta U_{\text{ex}}}{J} dJ. \quad (\text{A6})$$

Since the two phases have the same free energy, then  $\Delta U = l$  and hence we obtain the following expression for the slope quoted in the paper [Eq. (12)]:

$$\frac{dJ_c}{dT} = \frac{Jl}{T\Delta U_{\text{ex}}}. \quad (\text{A7})$$

<sup>1</sup>T. L. Jones and D. Venus, *Surf. Sci.* **302**, 126 (1994).

<sup>2</sup>M. Prutton, in *Introduction to Surface Physics* (Calarendon Press, Oxford, 1994).

<sup>3</sup>D. P. Pappas, K.-P. Kamper, and H. Hopster, *Phys. Rev. Lett.* **64**, 3179 (1990).

<sup>4</sup>R. Allenspach, M. Stampanoni, and A. Bischof, *Phys. Rev. Lett.* **65**, 3344 (1990).

<sup>5</sup>K. De'Bell, A. B. MacIsaac, and J. P. Whitehead, *Rev. Mod. Phys.* **72**, 225 (2000).

<sup>6</sup>P. I. Belobrov, R. S. Gekht, and V. A. Ignatchenko, *Zh. Éksp.*

*Teor. Fiz.* **84**, 1097 (1983) [*Sov. Phys. JETP* **57**, 636 (1983)].

<sup>7</sup>G. O. Zimmerman, A. K. Ibrahim, and F. Y. Wu, *Phys. Rev.* **37**, 2059 (1988).

<sup>8</sup>K. De'Bell, A. B. MacIsaac, I. N. Booth, and J. P. Whitehead, *Phys. Rev. B* **55**, 15 108 (1997).

<sup>9</sup>A. Carbognani, E. Rastelli, S. Regina, and A. Tassi, *Phys. Rev. B* **62**, 1015 (2000).

<sup>10</sup>A. B. MacIsaac, J. P. Whitehead, K. De'Bell, and P. H. Poole, *Phys. Rev. Lett.* **77**, 739 (1996). (See the comments in Ref. 5 regarding the sampling technique used in this paper.)

- <sup>11</sup>L. Corruccini and S. J. White, Phys. Rev. B **47**, 773 (1993).
- <sup>12</sup>C. Henley, Phys. Rev. Lett. **62**, 2056 (1989).
- <sup>13</sup>S. Prakash and C. L. Henley, Phys. Rev. B **42**, 6574 (1990).
- <sup>14</sup>J. P. Whitehead, Phys. Essays **9**, 609 (1996).
- <sup>15</sup>C. Pich and F. Schwabl, Phys. Rev. B **47**, 7957 (1993).
- <sup>16</sup>E. Vescovo (private communication).
- <sup>17</sup>T. W. Clinton, J. W. Lynn, J. Z. Liu, Y. X. Jia, and R. N. Shelton, J. Appl. Phys. **70**, 5751 (1991).
- <sup>18</sup>D. M. Paul, H. A. Mook, A. W. Hewat, B. C. Sales, L. A. Boatner, J. R. Thompson, and M. Mosteller, Phys. Rev. B **37**, 2341 (1988); H. A. Mook, D. M. Paul, B. C. Sales, L. A. Boatner, and L. Cussen, *ibid.* **38**, 12 008 (1988).
- <sup>19</sup>J. W. Lynn, T. W. Clinton, W.-H. Li, R. W. Erwin, J. Z. Liu, K. Vandervoort, and R. N. Shelton, Phys. Rev. Lett. **63**, 2606 (1989).
- <sup>20</sup>B. D. Dunlap, M. Slaski, Z. Sungaila, D. G. Hinks, K. Zhang, C. Segre, S. K. Malik, and E. E. Alp, Phys. Rev. B **37**, 592 (1988).
- <sup>21</sup>S. Simizu, G. H. Bellesis, J. Lukin, S. A. Friedberg, H. S. Lessure, S. M. Fine, and M. Greenblatt, Phys. Rev. B **39**, 9099 (1989).
- <sup>22</sup>T. W. Clinton, J. W. Lynn, J. Z. Liu, Y. X. Jia, T. J. Goodwin, R. N. Shelton, B. W. Lee, M. Buchgeister, M. B. Maple, and J. L. Peng, Phys. Rev. B **51**, 15 429 (1995).
- <sup>23</sup>K. De'Bell and J. P. Whitehead, Physica B **194-196**, 179 (1994).